Advanced Fault Detection of Synchronous Generators using Stray Magnetic Field

Hossein Ehya, *Student Member*, Arne Nysveen, *Senior Member*, and Jose. A Antonino-Daviu, *Senior Member*

***Abstract*—Many methods used for precise fault detection in salient pole synchronous generators (SPSGs) often require a priori knowledge of the healthy case, but this requirement impedes application of the methods since an accurate analysis of the different machine quantity waveforms is not usually carried out during commissioning. The inspection and maintenance processes in SPSGs are also costly and time-consuming; therefore, reliable methods that can detect and discriminate between different faults without comparison with the healthy condition are highly desirable. This paper proposes a precise method for detection and discrimination between different fault types in SPSG. The method does not require healthy machine data and is applied to diagnose both inter-turn short circuits (ITSC) in the field winding and dynamic eccentricities (DE). The proposed non-intrusive detection algorithm is based on advanced signal analysis of stray magnetic field data and can be applied during SPSG operation. The method is highly precise for monitoring the condition of the rotor field winding and yields a unique pattern for diagnosing possible ITSC faults. Moreover, a distinctive pattern for the DE fault enables the discrimination between both considered failures, even if they are present at the same time. The proposed method is validated through finite element modeling and experimentally on a 100 kVA and a 22 MVA SPSG to demonstrate its applicability in real power plants.**

***Index Terms*—Inter-turn short circuit, hydro power plant, fault detection, synchronous generator, condition monitoring, continuous wavelet transforms, reliability.**

I. Introduction

LARGE synchronous generators can be built with a salient pole concentrated excitation rotor or with non-salient pole distributed excitation rotors (cylindrical rotor) [1]. The former is typically used in low-speed generators or hydro generators, while the latter is employed in high speed turbo alternators. Cylindrical rotors in turbo alternators are usually based on solid iron rotors for better mechanical rigidity and heat transmission [1]. In lower speed synchronous generators, such as hydro generators, the rotor pole shoes are made by laminations to reduce rotor losses. In these low speed machines, the rotor pole shoes incorporate slots that house copper bars that are short-circuited by end rings to form the damper cage.

The salient pole synchronous generators (SPSG) in hydroelectric plants must operate in a sufficiently healthy condition due to the severe consequences of an eventual forced outage, not only for the plant itself but also for the electric system. Therefore, these machines are usually subjected to maintenance protocols that are much more exhaustive than those used in industrial synchronous motors. In this regard, specific condition monitoring systems, such as vibroacoustic sensors, internal search probes, thermal probes (PT100), or PD monitoring systems (e.g., stator slot couplers), are usually employed to guarantee accurate knowledge of the SPSG condition.

Despite the application of special maintenance protocols to synchronous machines, different types of failures have been reported in the literature for this type of machine. For example, broken damper bars have been reported both in salient pole synchronous machines and non-salient pole synchronous machines [2]–[6]. The number of reported broken damper bar failures in the synchronous motor compare with the synchronous generator is higher, however, faults due to broken dampers may have serious implications concerning the starting of synchronous machines [7]. Other faults, such as eccentricities [8], [9], shaft current discharges [10], and field winding [11] and stator turn faults [12], have also been reported in hydro generators. The negative effects of most of these failures can eventually lead to forced synchronous generator outages; therefore, an intensive effort has been devoted to the development of intelligent techniques that are able to detect these faults when they are in their early stages of development [11]–[13].

In this context, the analysis of flux data has been a recurrent alternative for the diagnosis of most of these faults. The basic idea relies on evaluating the signatures that the anomaly leaves, either on the waveform of the air-gap flux or on its frequency content. In this regard, air-gap flux analysis has been proposed to detect field winding failures [14], [15], damper faults [5], [16], eccentricities [17], or even stator turn faults. In spite of its good results, the air-gap flux has some important constraints related to the intrusive nature of the necessary sensors or to the reduced flexibility caused by the exclusive dependence on sensors that have already been installed during the manufacturing process. These sensors can be difficult to replace or modify in case of failure or when measurements in

This work was supported by the Norwegian Research Centre for Hydropower Technology (HydroCen) partly funded by The Research Council of Norway (contract no. 257588).

Hossein Ehya, and Arne Nysveen are with Department of Electrical Power Engineering, Norwegian University of Science and Technology, Trondheim, 7491, Norway. Jose. A Antonino-Daviu is with the Instituto Tecnologico de la Energia, Universitat Politecnica de Valencia, 46022 Valencia, Spain. (corresponding author phone: +47 47743322; e-mail: hossein.ehya@ntnu.no).

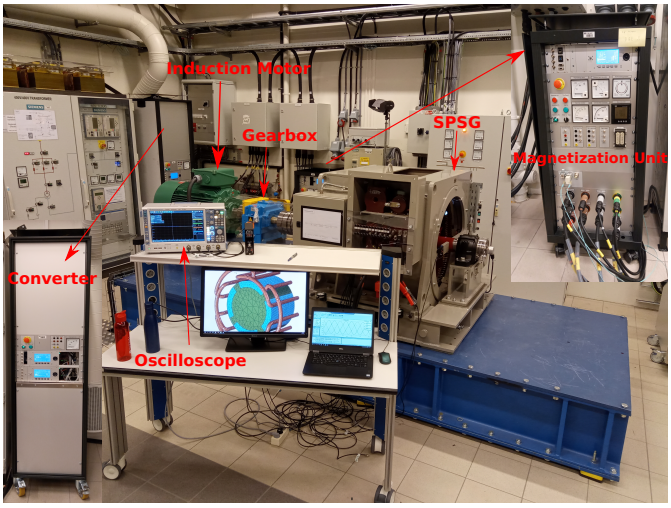

Fig. 1. The experimental setup of a 100 kVA salient pole synchronous generator.

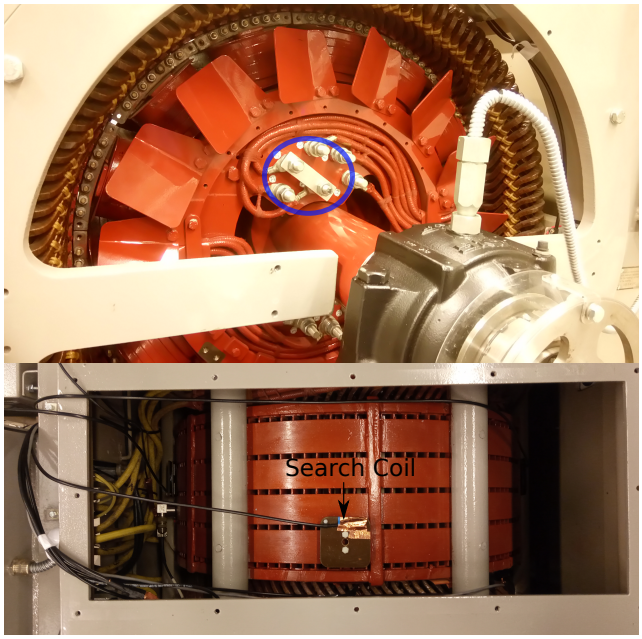

Fig. 2. The location of the shorted turns tap on the rotor (top) and the location of the stray magnetic field sensor installed on the stator back side of a SPSG.

alternative locations are required.

Due to these constraints, an emerging trend in recent years is to rely on the analysis of stray-flux data. Today, stray flux data can be acquired in a non-invasive way using the currently available sensors with advanced features [18]. Several studies have confirmed the validity of the technique for diagnosing faults in induction motors and even in permanent magnet machines [19]. In addition, new techniques based on the advanced analysis of stray flux data under transient conditions have been confirmed to provide important advantages when compared with the analysis of stationary flux signals [20]–[22].

Some recent work has suggested the analysis of stray flux data for the detection certain faults in SPSGs, such as field winding faults [23], [24], damper faults [24], [25], eccentricities [9], [26] or even stator faults [27]. This work has verified the potential of this technique for reliable detection of these faults and for their discrimination from other faults or non-faultârelated phenomena. Despite this, further research work is still required in this area to develop alternative methods that are effective in real SPSG operating in power plants.

In this context, this work proposes a precise stray flux-based method to diagnose inter-turn short circuit faults (ITSC) and parallel dynamic eccentricities (DE) in an SPSG. The application of the proposed methods yields characteristic signatures that are specific to each type of failure, thereby enabling their respective detection and discrimination. The effectiveness of the method is proven both with simulated data and with laboratory and field test data obtained in a 100 kVA and 22 MVA SPSG operating in a hydropower plant. Application of the approach enabled the avoidance of an eventual catastrophic failure thanks to the early detection of the faults. This paper first presents the laboratory and field tests in which the fault effects on the captured stray flux signals are observed. This is followed by the justification of these observations, both by simulations with finite element models and by advanced time-frequency analyses of the experimental data.

II. Laboratory and Field Test

A. Laboratory Setup

Numerous tests were performed in the laboratory on a 100 kVA SPSG. The objective was to obtain the corresponding stray flux signals and to observe their corresponding waveforms that could be indicative of certain faults. These waveforms are processed later, and the observed phenomena are properly described and justified via time-frequency analyses. A detailed description of the experimental setup, as shown in Fig. 1, is as follows:

1) A 100 kVA, 400 V custom-made synchronous generator with 14 salient poles is used to investigate the ITSC fault in the rotor field winding.
2) A 100 kVA induction motor with four poles is used as a prime mover of the SPSG.
3) The SPSG and induction motor are connected using a gearbox with a gear ratio of four to one.
4) A 100 kVA converter is used to drive the induction motor and to provide the SPSG with the required active power at constant speed.
5) A static rotor magnetization unit is used to control the current in the rotor field winding. Controlling the power field excitation is possible both in a local mode while the generator is connected to the passive loads or when it is integrated into the power grid.
6) A stray magnetic field is recorded by a homemade sensor that consists of an air-core coil with 3000 turns of thin copper wire (0.12 mm^2). The sensor can be attached both on the stator backside to pick up the radial stray flux and in front of the stator end winding to pick up the axial stray flux. The sensor picks up both axial and radial stray flux if it is tangentially attached to the stator backside as shown

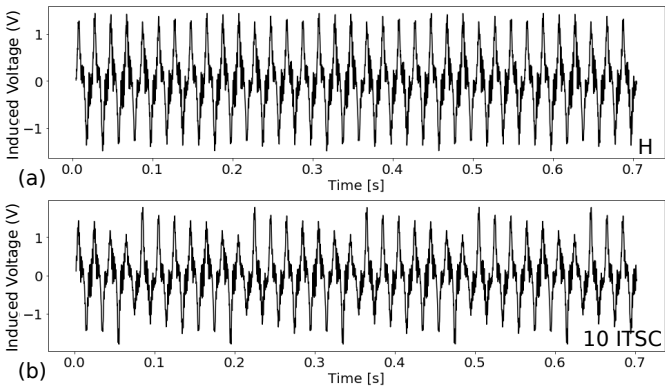

Fig. 3. Induced voltage due to a stray magnetic field in the sensor attached on the stator back side of a 100 kVA SPSG during no-load operation in a healthy case (a) and under a 10 ITSC fault (b) - Laboratory measurements.

in Fig. 2. The size of the sensor is optimized to cover an adequate area of the stator back side ($100 \times 100 \times 10$ mm).

7) A high-resolution 16-bit oscilloscope (Rohde Schwarz RTO2000) is used to sample the stray magnetic field using a sampling frequency of 10 kHz.
8) The ITSC fault on one of the rotor pole windings is created by removing the desired number of turns. Removal of 1, 2, 3, 7, or 10 turns from one of the rotor poles is possible using a copper plate, as shown in Fig. 2.

B. Laboratory Measurement

The procedure for experimental measurement is as follows: a copper plate is mounted between the common point of the rotor pole winding and the desired tap of the rotor pole winding to remove the specific turns in the standstill. The SPSG is then accelerated until it reaches the synchronous speed. The DC current is then applied to the field winding based on the loading condition.

Fig. 3 shows the waveforms of the induced voltage in the sensor attached on the stator back side of the 100 kVA SPSG for the healthy and the ITSC fault condition. A clear variation exists in the amplitude of the induced voltage under a 10 ITSC fault compared with the healthy case. Each mechanical revolution consists of seven periods that are in concordance with the number of pole pairs in the laboratory machine. The pattern arises because the ITSC fault in the rotor field winding is periodic as long as the rotor passes over the installed sensor on the stator back side. The reduction in the amplitude of the induced voltage under the ITSC fault is due to the reduced number of turns in the faulty rotor field winding that contribute to the magneto-motive force in the air-gap.

C. Field Test Measurement

Fig. 4 shows a 22 MVA, synchronous generator with a 8 salient poles operating in a Norwegian hydropower plant. Several inspections had revealed a clear elevation in the measured amplitude of the vibration according to the power plant report. Therefore, measurement of the stray magnetic

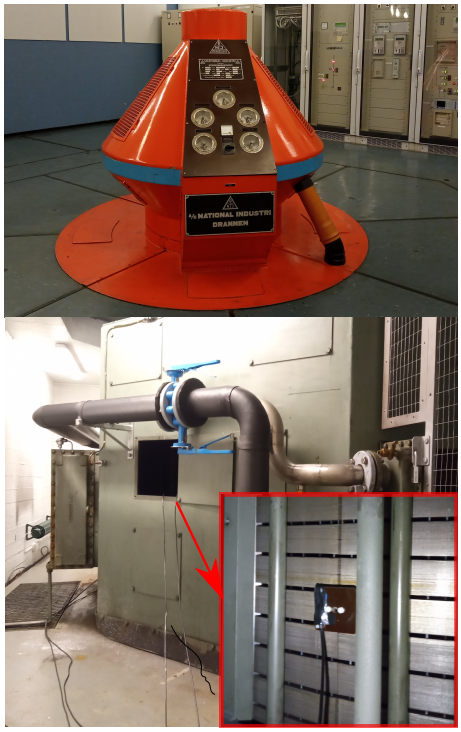

Fig. 4. A single unit hydropower plant with an operating 22 MVA SPSG.

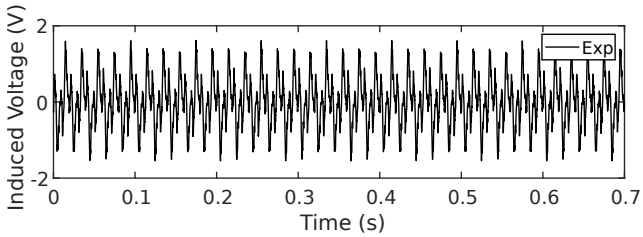

Fig. 5. Induced voltage in the installed sensor on the stator back side of a 22 MVA SPSG during no-load operation - Field test measurement.

field was proposed to determine the origin of this symptom. The SPSG was completely covered by an iron housing, but several hatches enabled access to the stator yoke back side. Fig. 4 shows the installed sensor on the stator yoke through one of the hatches. At least four sensors are required to detect a static eccentricity fault in a vertically mounted SPSG, while one sensor is adequate for ITSC fault and DE fault diagnosis. However, since the type of fault in the SPSG is unknown, four sensors were installed at a distance of 90 mechanical degrees.

Fig. 5 shows the induced voltage in one of the installed sensors on the stator back side of a 22 MVA SPSG. A clear sign of amplitude variation is evident in the induced voltage. The amplitude reduction of the induced voltage shows an obvious pattern that is similar to the pattern in the100 kVA SPSG, whereas a significant difference is detected in the lower envelope of the signal, since the envelope of the signal does not follow the pattern expected for an ITSC fault. The lower envelope of the induced voltage, in this case, is similar to a sine wave. This indicates that, in addition to the ITSC fault, another source is generating the fault in the 22 MVA SPSG.

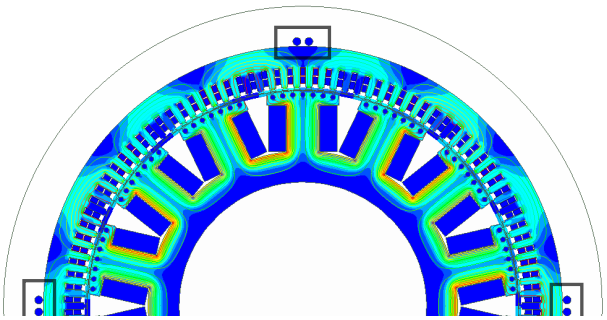

Fig. 6. Finite element model of a 100 kVA SPSG and the location of the stray magnetic field sensor installed on the back side of the stator yoke.

TABLE I
100 kVA, 50 Hz, SYNCHRONOUS GENERATOR TOPOLOGY SPECIFICATION AND NAMEPLATE DATA

Quantity	*Values*	*Quantity*	*Values*
Stator outer diameter	780 mm	Number of poles	14
Stator inner diameter	649 mm	Nominal exc. current	103 A
Length of stack	208 mm	Power factor	0.90
No. of damper bars/pole	7	Terminal current	144.3 A
No. of rotor turns / pole	35	Terminal voltage	400 V
No. of stator turns	8	No. of slots	114
Nominal speed	428 rpm	Winding connection	Wye

The amplitudes of the signals captured by the four sensors installed with a mechanical distance of 90 degrees are checked to inspect the possibility of a static eccentricity fault. The amplitude of one pair of sensors installed in front of each other must differ in a way that ensures that the amplitude of the induced voltage in one of the sensors is high and that of the other sensor is low for a static eccentricity fault to occur [9]. However, the amplitudes of the induced voltages in this pair of sensors are similar, which indicates the absence of a static eccentricity fault in the 22 MVA SPSG.

III. ELECTROMAGNETIC ANALYSIS

The aim of this section is to evaluate the impact of different faults on the stray magnetic field distribution of the SPSG. Two SPSGs with power ratings of 100 kVA and 22 MVA are modeled by considering two types of faults: ITSC and DE. The pattern of the voltage signal induced in the sensor by the stray magnetic field is analyzed to determine the impact of both failures under consideration. The occurrence of both ITSC and DE faults results in the magnetic field variation in the air gap. The magnetomotive force of the faulty rotor pole compared with the healthy poles decreased due to the reduced number of turns. The reduced magnetomotive force affects the symmetry of the air-gap magnetic field and consequently its amplitude. DE fault also disturbs the air-gap magnetic field symmetry distribution in the air-gap. Therefore, in the case of both faults, the reluctance of the path between the air gap and the search coil starts to change. The reluctance variation results in the leakage flux variation and consequently the induced voltage variation in the sensor due to the faults.

Both the detailed specification of the SPSG geometry and the non-linearity of the material are considered in finite element modeling (FEM), since both have a marked impact on the stray flux distribution. The eddy effect in damper bars is also considered since a synchronous machine with a fractional winding layout has a circulating current in the damper bars even during steady-state operation [4]. A 2D FEM model of the SPSGs is adequate since the rotor or damper bars are not skewed. The complete geometry is required for FEM, since both machines have a fractional slot winding layout; therefore, both ITSC and DE result in an asymmetric distribution of the magnetic field. The simulation is performed using the ANSYS ELECTRONICS software package [28].

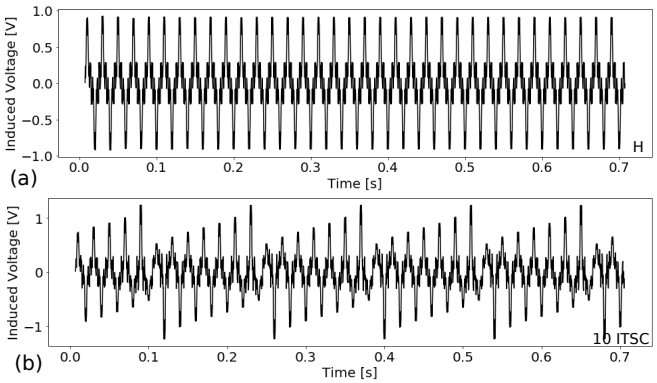

Fig. 7. Induced voltage in the sensor installed on the stator back side of a 100 kVA SPSG operating in a no-load in a healthy case (a) and under a 10 ITSC fault (b) - Simulation results.

A. FEM Study of a 100 kVA SPSG

A 100 kVA, 400 V, star-connected SPSG with 14 poles (each pole including 7 damper bars) and with 114 stator slots is modeled in FEM, as shown in Fig. 6. The detailed specifications of the 100 kVA SPSG are shown in Table I. The rotor field winding of each pole has 35 turns. The analysis is performed for five different severities of an ITSC fault in the rotor field winding: 10 shorted turns (28.57%), 7 shorted turns (20%), 3 shorted turns (8.5%), 2 shorted turns (5.7%), and 1 shorted turn (2.85%). The corresponding number of turns in each rotor pole is eliminated in order to model the ITSC fault with FEM. Therefore, the effective magneto-motive force decreases, which results in a non-uniform air gap magnetic field.

Fig. 7 shows the calculated induced voltage in the sensor installed on the stator back side of the simulated SPSG in the FEM for both a healthy case and for a 10 ITSC fault. A symmetrical pattern is evident in the healthy operation of the machine, whereas the pattern is distorted by the 10 ITSC fault (see bottom row of Fig. 7). The amplitude of the induced voltage is decreased when the faulty rotor pole passes over the sensor installed on the stator back side. A comparison between the experimental measurements, shown in Fig. 3, and the simulation results, depicted in Fig. 7, proves that the ITSC fault causes a reduction in the effective magneto-motive force and, consequently, a decrease in the stray magnetic field in the vicinity of the stator yoke. The shape, periodicity, and pattern are the same for both the experimental results and the FEM results; however, the direction of the peak amplitude reduction differs due to the polarity of the installed sensor.

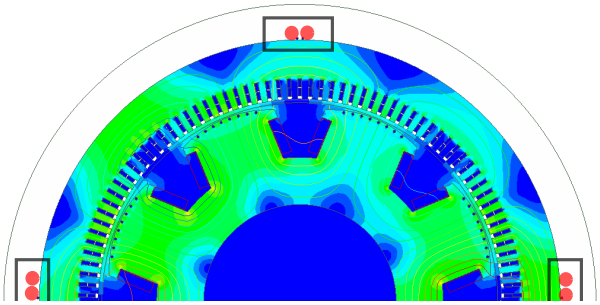

Fig. 8. Finite element model of the 22 MVA SPSG and the location of the installed stray magnetic field sensor.

TABLE II
22 MVA, 50 Hz, SYNCHRONOUS GENERATOR TOPOLOGY SPECIFICATION AND NAMEPLATE DATA

Quantity	*Values*	*Quantity*	*Values*
Stator outer diameter	2640 mm	Number of poles	8
Stator inner diameter	2040 mm	Nominal exc. current	440 A
Length of stack	1220 mm	Power factor	0.90
No. of damper bars/pole	8	Terminal current	1650 A
No. of rotor turns / pole	58	Terminal voltage	7700 V
No. of stator turns	1	No. of slots	126
Nominal speed	750 rpm	Winding connection	Wye

B. FEM Study a 22 MVA SPSG

The FEM model of the 22 MVA SPSG is illustrated in Fig. 8. Table II shows the detailed specifications of the machine. The generator has 8 poles, and each pole contains 8 damper bars. The required magneto-motive force to generate 7.7 kV on the stator terminals is provided by 53 turns in each rotor field winding. The stator windings are connected in series and, unlike a generator with a parallel winding layout, they do not yield a circulating current to compensate for the asymmetric magnetic field caused by a short circuit fault or eccentricity fault. Two pairs of sensors are installed exactly in front of each other, and the amplitude of the induced voltage in all the sensors was the same, indicating that the SPSG does not have a static eccentricity fault. Consequently, only the DE and ITSC faults are simulated in FEM.

A comparison between the simulation result and the measurement in the power plant shows the accuracy of the FEM model; only a small difference is apparent in the shape of the signal, and this difference is due to ignoring the 3D effect and the radial air duct effect, as well as the SPSG housing. The impact of a 20% DE fault on the induced voltage in the sensor is shown Fig. 9. A periodic fluctuation occurs in both the upper and lower envelopes of the signal due to the DE fault. Conversely, the effect of the ITSC fault on the induced voltage of the sensor also results in a reduction in the peak amplitude, as indicated in green in the plot shown in Fig. 9. However, a comparison between the measured voltage in Fig. 5 and the FEM results under only an ITSC or DE fault indicates that both ITSC and DE faults exist simultaneously in the 22 MVA SPSG. The last plot of Fig. 9 shows the simultaneous occurrence of a 10 ITSC and a 20% DE fault. The obtained pattern for this mixed fault is a combination of the fault-related patterns of both the ITSC and DE faults, since the upper envelope is similar to the upper envelope of the ITSC fault and the lower envelope is similar to the DE fault.

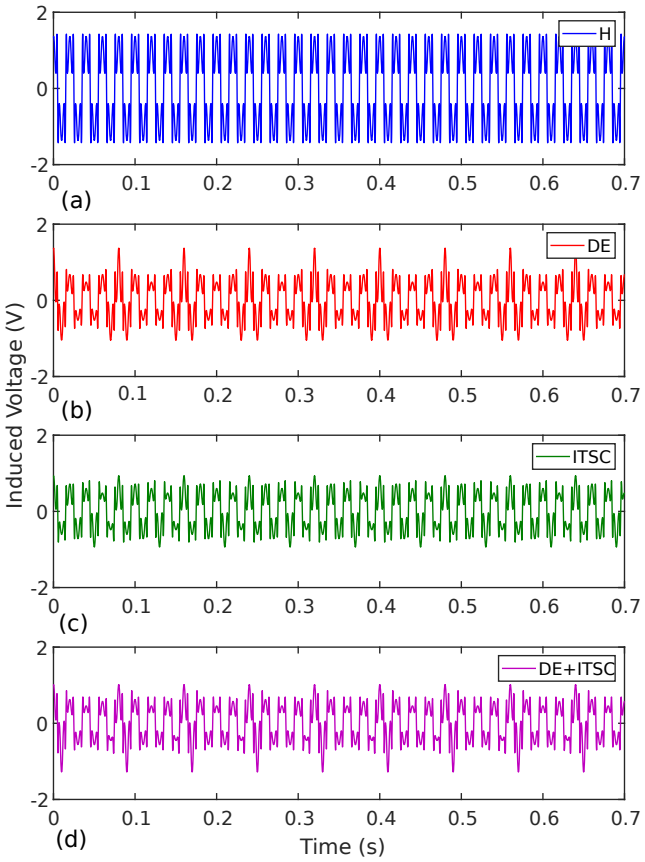

Fig. 9. Measured induced voltage in a sensor installed on the stator back side of a 22 MVA SPSG operating in a no-load in a healthy case (a), under a 20% DE fault (b), under a 10 ITSC fault (c), and under a combination of both DE and ITSC faults (d) - Simulation results.

IV. ADVANCED SIGNAL PROCESSING

Digital signal processing is a broad field that encompasses numerous mature techniques for treating a signal and extracting useful information based on the required needs. Several signal processing tools are available, and these can be classified, according to their application in fault detection of electrical machines, into three categories including time-domain, frequency-domain, and time-frequency domain tools. The application is based on the signal properties and the required format for data interpretation. Application of fast Fourier transforms to the induced sensor voltage in a healthy case and under ITSC and DE fault is presented in Fig. 10. Although the faulty frequency spectrum demonstrates the significant increase in the amplitude of both sub-harmonics and inter-harmonics, both faults intrigue the same fault harmonic components. Indicating that fault type detection using frequency spectrum is impossible. This paper proposes a time-frequency representation of the voltage induced in the sensors installed on the stator back side and uses the continuous wavelet transform (CWT) as a time-frequency tool. The Gaussian mother wavelet is selected based on the signal

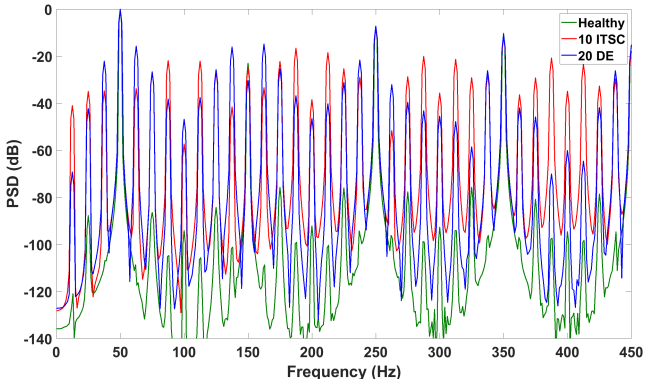

Fig. 10. The frequency spectrum of the sensor induced voltage in a 22 MVA SPSG operating at no-load in a healthy case and under 10 ITSC and 20% DE faults - Simulation results.

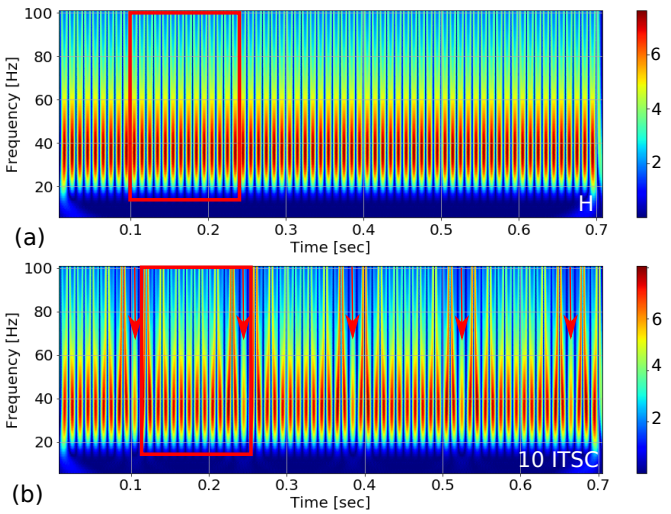

Fig. 11. Time-frequency representation of the induced voltage in the a sensor installed in a 100 kVA SPSG operating in a no-load in a healthy case (a) and under a 10 ITSC fault (b) - Simulation results

characteristics. The frequency band is assigned to 100 Hz and the window length must be selected to have at least two mechanical revolutions in order to exhibit the periodicity of the fault signature.

CWT is a powerful tool for analyzing localized variations of power spectral density within a time data series. Wavelet transforms decompose the time data series into a time-frequency map that enables determination of both the dominant modes of variability and how the modes vary in time. Implementation of the CWT, compared with other tools like the Discrete Wavelet Transform (DWT), is also straightforward since a mother wavelet is constructed simply by dilating and translating the signal. The frequency component of the signal is extracted using a convolution process, and the transform convolutes the signal with a wavelet instead of running the Fourier transform [29].

One of the main concerns of fault detection methods proposed in several published studies is their prerequisite for knowledge of the healthy condition of the SPSG. This requirement can be easily satisfied under laboratory conditions, where the fault is applied intentionally and the healthy data are accessible. However, this is not the case for machines in real power plants. Consequently, some methods proposed in the literature, although suitable in principle for SPSGs, are difficult to apply in the field. The method proposed in this paper, based on CWT, extract a clear pattern that reveals the SPSG health status without requiring any knowledge of the healthy operation data.

V. Results and Discussions

Although the obtained time data series results have a clear pattern indicating the occurrence of the fault in both the 100 kVA and the 22 MVA SPSG, an advanced signal processing tool, such as CWT, can be used to support the findings and identify the amplified frequency components. The following two sections include analyses of the voltage induced in the sensor in the healthy and faulty cases for simulations, laboratory experiments, and field tests.

A. Study Results of a 100 kVA SPSG

Fig. 11 shows the CWT results of the voltage induced in the sensor by a stray magnetic field for the healthy condition and for a 10 ITSC fault in the field winding, using simulated data obtained with FEM. The time-frequency analysis of the induced voltage yields numerous stalks, each corresponding to one rotor pole. The 100 kVA SPSG has 14 poles that yield 14 stalks for each mechanical revolution, as shown in Fig. 11. The frequency range of each stalk for a healthy case spans from 20 Hz to 100 Hz. The presence of a 10 ITSC fault in one of the rotor field windings reduces the magneto-motive force produced by a faulty pole, thereby influencing the stray magnetic field on the stator yoke back side. The time-frequency plot of the induced voltage for the 10 ITSC fault reveals a significant reduction in the stalk length and intensity, indicating a faulty rotor pole winding (red arrows designate a faulty pole). The time-frequency plot contains five mechanical revolutions of the 100 kVA SPSG. Each time a faulty pole passes over the sensor, a faulty pole with a reduced stalk length appears in the time-frequency plot.

The application of the CWT to the experimental data of a 100 kVA is shown in Fig. 12 for a healthy case and a 10 ITSC fault. The time-frequency plot for the healthy case is similar to that of Fig. 11; each 140 ms indicates one mechanical revolution with 14 stalks, which is evidence of a healthy rotor pole winding. Although the results of analysis are similar for the experimental data corresponding to the faulty machine and for the simulation data, the stalk length is (negligibly) shorter for the experimental result than for the simulation result. Therefore, the stalk length of a faulty pole spans slightly above 20 Hz, making the identification of a faulty pole more noticeable in practice.

B. Study Results of a 22 MVA SPSG

The identified fault types in a 22 MVA SPSG according to the FEM results are both the ITSC and DE, as verified based

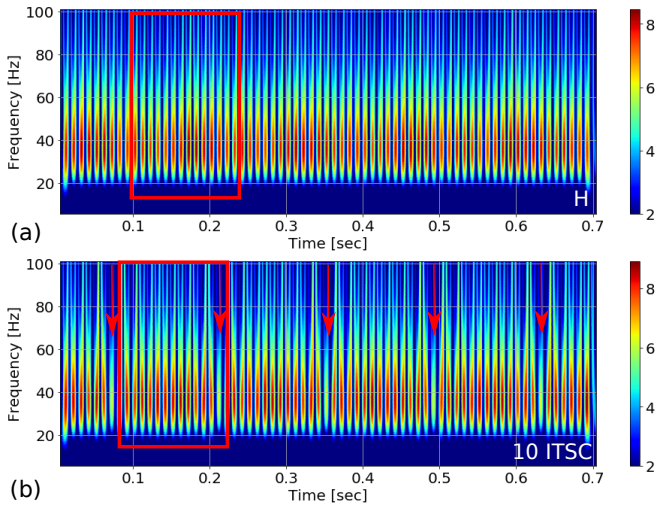

Fig. 12. Time-frequency representation of the induced voltage in the a sensor installed in a 100 kVA SPSG operating in a no-load in a healthy case (a) and under a 10 ITSC fault (b) - Laboratory measurements.

on the time-frequency presentation of the induced voltage both in field measurement tests and FEM. Fig. 13 shows the application of the CWT to the voltage induced by the stray magnetic field for the healthy condition (first row), 10 ITSC fault (second row), 20% DE fault (third row), and mixed fault of 10 ITSC and 20% DE faults. The 22 MVA SPSG has 8 poles, shown in the red window in Fig. 13; the stalk frequencies are set between 20 Hz and 100 Hz to have high resolution in the time-frequency plot. The highest stalk intensity concentrated in the 25-60 Hz range with a red hue. The 20% DE fault causes a time-frequency pattern modification. Three changes occur due to the DE fault in the time-frequency plot compared with the healthy case:

- A fluctuating envelope appears at the bottom of the time-frequency plot, similar to the time data series shown in Fig. 9.
- The healthy case shows a uniform distribution in the time-frequency plot, whereas the 20% DE fault shows a distorted distribution, with each window shape resembling a fire flame.
- The intensity of the stalks in the healthy case are the same for each mechanical revolution, as is the frequency range, whereas the 20% DE fault modifies the intensity pattern, with the highest intensity located in the middle of the window and a reduction in the stalk intensity at the edges.

A 10 ITSC fault reduces the stalk intensity of faulty pole in the time-frequency plot. The starting frequency point of each faulty stalk is slightly higher than 25 Hz, unlike a healthy stalk. Fig. 13 shows the time-frequency plot of an induced voltage in the sensor for a 22 MVA SPSG operating under simultaneous ITSC and DE faults. The expected pattern for ITSC fault and DE fault must appear in the time-frequency plot. Therefore, the fire flame shape pattern with a sine shape envelope at the bottom of the plot appears which indicates the occurrence of DE fault. A comparison between the length of the stalks in the time-frequency plot of a DE fault indicates

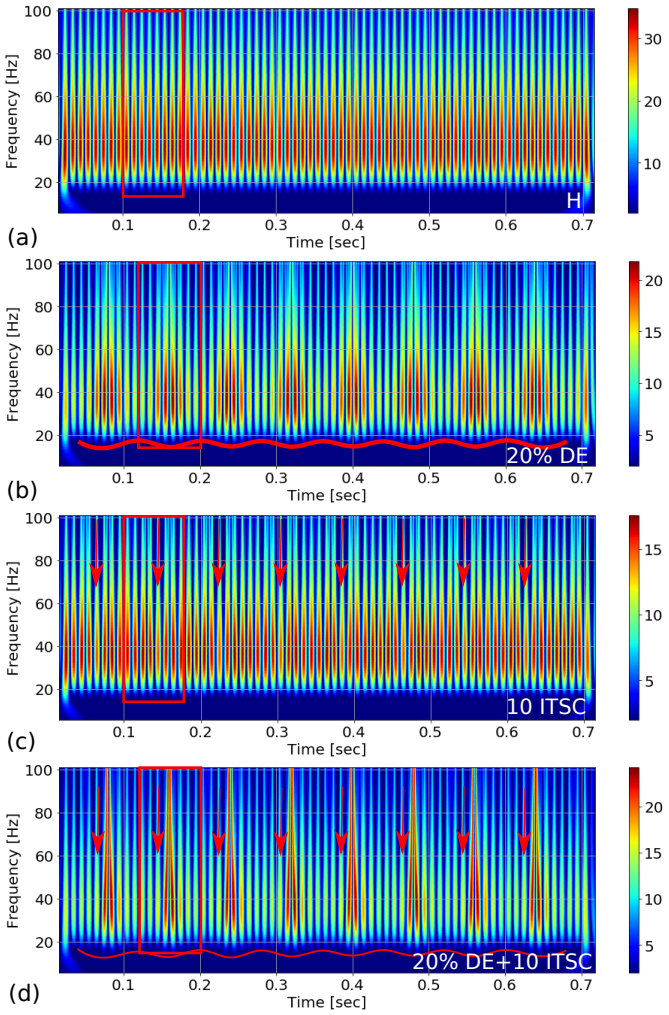

Fig. 13. The simulation result of the time-frequency representation of the induced voltage in the installed sensor on a 22 MVA SPSG operating in a no-load in a healthy case (a), under a 20% DE fault (b), under a 10 ITSC fault (c), and under mixed fault of 20% DE and 10 ITSC fault (d) - Simulation results.

that there is a symmetry in the length of the stalks with respect to the window center. The existence of ITSC fault while the machine has DE fault results in the length reduction in one of the stalks which can be detected by comparing the length of opposite stalk.

Fig. 14 shows the time-frequency presentation of the measured voltage induced in an installed sensor in a 22 MVA SPSG in a hydropower plant operating under no load (top row) and under a 17 MW load (bottom row). The patterns suggest a combination of both ITSC and DE faults and are interpreted as follows:

- A DE fault is indicated by the fluctuating envelope at the bottom, the flame shape of each mechanical revolution, and the concentrated high intensity of the stalks at the center of the window in the time-frequency plot.
- The frequency ranges of one of the stalks are initiated slightly higher than for a healthy winding stalk. The stalk intensity that shows the ITSC fault in a rotor winding is low compared to the rest of the neighboring stalks.

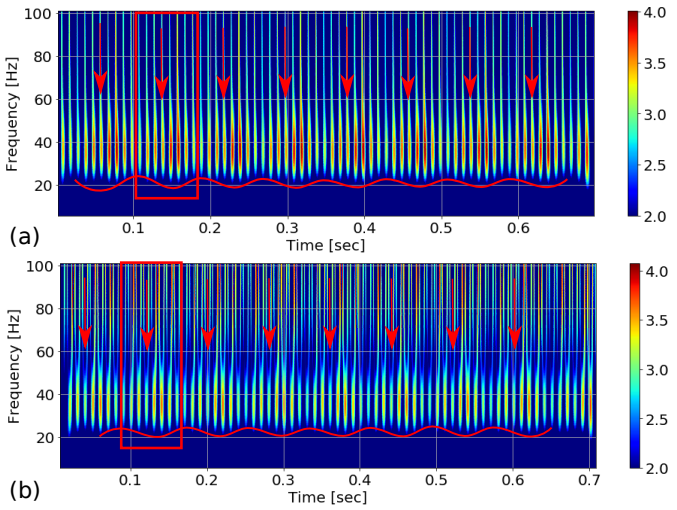

Fig. 14. The time-frequency representation of the induced voltage in a sensor installed in a 22 MVA SPSG in a no-load operation (a) and under loaded operation of 17 MW (b) - Field test results.

C. Load impact

The SPSG in hydropower plants always operates under different loading conditions, indicating that the load impact on the proposed method must be investigated. The main difference between the no-load and loading condition is the contribution of the stator magnetic field due to the current in the stator windings. The stator magnetic field has two impacts on the stray magnetic field. The magnitude of the stray magnetic field is slightly increased compared with the no-load case. The stray magnetic field in the loading condition has a phase shift compared with the no-load case. However, the frequency contents of the stray magnetic field do not change due to loading conditions. Therefore, the introduced pattern due to the loading condition of SPSG must stay unchanged while its intensity due to increment in the amplitude of the stray magnetic field must be changed.

The ITSC and DE faults pattern in the time-frequency plot is more noticeable in a loaded SPSG than in a no-load SPSG, as shown in Fig. 14. The reason is that the amplitude of the current in the rotor field winding increases by increasing the load in the SPSG; therefore, the impact of reduced contributing magnetomotive force from the faulty pole in the air-gap magnetic field and correspondingly in the stray magnetic field becomes more tangible. Consequently, the intensity of the faulty stalk due to an ITSC fault is markedly reduced under the 17 MW load. Conversely, the electromotive force of the faulty pole is decreased compared with the healthy poles therefore, increasing the current reduces the magneto-motive force due to the ITSC fault. The power plant operator also stated that the amplitude of the vibration increased during loading conditions, possibly due to the ITSC fault. The DE pattern in the time-frequency plot under the loading condition does not change because the winding layout is not parallel; parallel windings would compensate for the non-uniform magnetic field caused by the fault.

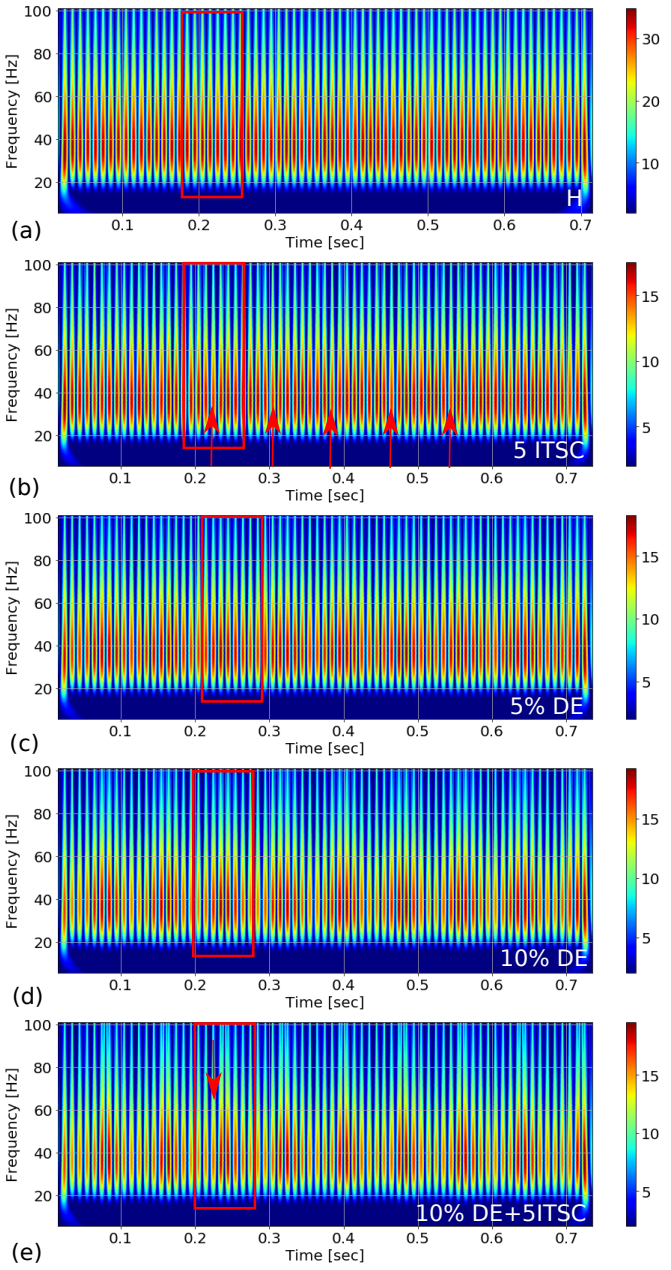

Fig. 15. The time-frequency representation of the sensor induced voltage in a 22 MVA SPSG operating at no-load in a healthy (a), under a 5 ITSC fault (b), under 5% DE fault (c), under 10% DE fault (d) and under mixed fault of 10% DE and 5 ITSC faults (e) - Simulation results.

D. Generalization of the method

The proposed method has a high sensitivity to detect the fault in an early stage. The lowest ITSC fault and DE fault that can be detected with a visual inspection of the time-frequency plot is shown in Fig. 15. The ITSC fault is applied to a 22 MVA SPSG by removing 5 turns out of 58 turns in one of the rotor field winding. The length and the intensity of the faulty stalk in the time-frequency map are decreased as shown in Fig. 15. DE fault with 5% and 10% severity is also applied to the 22 MVA SPSG and the same pattern for a severe fault such as 20% DE fault is observed for the low severity fault. The introduced pattern is able to detect the coexistence of

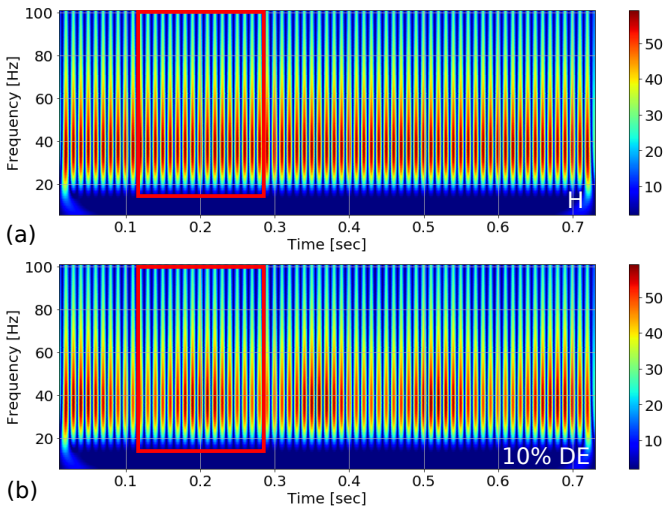

Fig. 16. The time-frequency representation of the sensor induced voltage in a 42 MVA, 16 poles SPSG operating at no-load in a healthy (a) and under 10% DE fault (b) - Simulation results.

ITSC fault and DE fault in an early stage as shown in Fig. 15. The fire flame pattern due to DE fault in the symmetrical at the middle of the window while having ITSC fault change the symmetry due to the reduced length and intensity of the faulty stalk.

The proposed method in this paper only requires the number of poles in the SPSG and the machine configuration does not have any impact on the introduced pattern. Fig. 16 shows the time-frequency map of a sensor induced voltage in a 42 MVA synchronous generator with 16 salient poles in the rotor. The red window Fig. 15 shows one mechanical revolution of the 42 MVA SPSG that includes 16 stalks which represent 16 poles. The introduced pattern for DE fault is observed in Fig. 16 where 10% DE fault is applied to the SPSG. Conclusively, the SPSG topology does not have any influence on the introduced pattern based on the application of CWT to the induced voltage in the sensor installed on the stator backside.

The method provided in this paper has several advantages and some limitation compared with the previously developed methods as follows:

1) ITSC and DE faults detection based on the application of FFT on the stray magnetic field in a SPSG are proposed in [9], [30]. The method compares the frequency spectrum of the faulty SPSG with a healthy SPSG in order to determine the health status of the machine. Although the method is able to detect the fault at an early stage since the frequency contents of a faulty machine are increased compared with a healthy machine, the frequency spectrum is unable to determine the fault type. The intrigued frequency components due to ITSC and DE fault are similar, indicating that the fault type recognition is impossible while the proposed method in this paper can detect the fault type based on unique patterns for DE and ITSC faults.
2) A method based on the application of STFT is proposed to detect ITSC and DE fault in SPSG using stray magnetic [31]. Although the method was able to introduce a new pattern that can detect the fault at an early stage, the pattern for DE and ITSC fault were similar that makes fault type detection difficult.
3) A highly sensitive method using DWT is proposed to detect the DE fault based on the differential stray magnetic field [9]. In this method, at least two sensors are required to embed on the stator core exactly opposite of each other. The measured signals are differentiated and processed by DWT. The method assumes that the differential signal is almost zero for a healthy SPSG. However, the assumption is incorrect since the induced sensor voltage is not identical even in the healthy SPSG due to asymmetry in the machine structure.
4) The proposed methods based on frequency spectrum are highly sensitive to the noise while the methods based on time-frequency methods such as STFT, and CWT is highly robust to the noise in the data sets [32].

Although the proposed method in this paper has several merits that make it practical especially in the field, there exist some constraints as follows:

1) A high-resolution signal can be achieved if the sensor is mounted on the stator core. The SPSG frame can significantly attenuate the stray magnetic field.
2) The sensor design must be optimized based on the stray magnetic field type, the strength of the stray magnetic field, and the sensor location.
3) The sensor must be shielded and a co-axial cable must be used to transfer the data in order to reject the noise impact.
4) The data acquisition system with at least 16-bit resolution is required for fault detection based on the stray magnetic field.
5) Although the proposed method can be easily utilized by the end-user since the pattern for each fault type is unique, the application of a deep neural network in pattern recognition can facilitate automate fault detection.

VI. Conclusion

This paper has presented a unique methodology for the detection of both ITSC and DE faults in a SPSG by applying CWT to the induced voltage in a flux sensor installed on the stator yoke back side. When compared with previously proposed methods for the detection of ITSC and DE faults, the detection algorithm in this paper has the following advantages:

- No a priori knowledge of the healthy operation of the SPSG is required because the time-frequency plot provides an informative and reliable pattern for fault detection.
- The method can identify and discriminate fault types with high accuracy based on the obtained time-frequency patterns. The occurrence of the ITSC fault in one rotor field winding causes a reduction of the stalk length, whereas a DE fault yields an envelope at the bottom of the time-frequency plot and each mechanical revolution of the machine resembles a fire flame.
- The non-intrusive nature of the method, based on stray magnetic field monitoring that induces a voltage in installed sensors on the stator back side, allows assessment

even during machine operation. Unlike previously proposed methods, it does not require machine stoppage or access to its internal parts.
- The proposed method is applicable to different types of SPSGs. The only required information is the number of poles.

The FEM provides insight into the changes in time-frequency patterns due to ITSC and DE faults in 100 kVA and 22 MVA SPSGs when CWT is applied. The experimental results for a small-scaled 100 kVA SPSG verified the feasibility of the methodology to detect an ITSC fault. The proposed method is able to detect and discriminate a co-existing ITSC fault and DE fault in a 22 MVA SPSG operating in one of the Norwegian hydropower plants under a no-load or a loaded condition, supporting the feasibility of this method in real power plants.

REFERENCES

[1] I. Boldea, *Synchronous generators*. CRC press, 2015.

[2] J. Bacher, "Detection of broken damper bars of a turbo generator by the field winding," *Renewable Energy Power Quality Journal*, vol. 1, no. 2, pp. 199–203, 2004.

[3] G. Ebi, "Ageing generator rotor: Refurbishment or removal from service?" *Power Engineering International*, vol. 17, 2009.

[4] H. Ehya and A. Nysveen, "Comprehensive broken damper bar fault detection of synchronous generators," *IEEE Transactions on Industrial Electronics*, DOI 10.1109/TIE.2021.3071678, pp. 1–1, 2021.

[5] H. Karmaker, "Broken damper bar detection studies using flux probe measurements and time-stepping finite element analysis for salient-pole synchronous machines," in *4th IEEE International Symposium on Diagnostics for Electric Machines, Power Electronics and Drives, 2003. SDEMPED 2003.*, pp. 193–197. IEEE, 2003.

[6] A. Schwery, "Large hydro generators experience and references," in *CIGRE session*, 2008.

[7] J. Antonino-Daviu, V. Fuster-Roig, S. Park, Y. Park, H. Choi, J. Park, and S. B. Lee, "Electrical monitoring of damper bar condition in salient-pole synchronous motors without motor disassembly," *IEEE Transactions on Industry Applications*, vol. 56, no. 2, pp. 1423–1431, 2020.

[8] Q. Sun, C. Ma, S. Xiao, L. Niu, J. Pu, and Y. Wu, "Analysis of influence of uneven air gap of hydrogenerator on magnetic field strength and rotor magnetic pole stress change," in *2020 IEEE International Conference on Energy Internet (ICEI)*, pp. 147–151. IEEE, 2020.

[9] R. N. Hossein Ehya, Arne Nysveen and Y. Liu, "Static and dynamic eccentricity fault diagnosis of large salient pole synchronous generators by means of external magnetic field," *IET Electric Power Applications*, vol. n/a, DOI https://doi.org/10.1049/elp2.12068, no. n/a. [Online]. Available: https://ietresearch.onlinelibrary.wiley.com/doi/abs/10.1049/elp2.12068

[10] O. Blancke, A. Merkhouf, N. Amyot, J. Pedneault-Desroches, C. Hudon, and K. Haddad, "Strategic fault diagnosis approach for hydrogenerator shaft current discharges," in *2016 XXII International Conference on Electrical Machines (ICEM)*, pp. 2346–2351. IEEE, 2016.

[11] A. Mugarra, C. Platero, J. Martínez, and U. Albizuri-Txurrka, "Large salient pole synchronous machines field windings diagnosis by frequency response," in *2018 XIII International Conference on Electrical Machines (ICEM)*, pp. 1875–1880. IEEE, 2018.

[12] W. Hong and M. Arshad, "Experience with hydro-generator turn-to-turn insulation fault, investigation, and recommendation for new stator winding design and protection," in *2018 IEEE Electrical Insulation Conference (EIC)*, pp. 459–464. IEEE, 2018.

[13] H. Ehya, T. Skreien, and A. Nysveen, "Intelligent data-driven diagnosis of incipient inter-turn short circuit fault in field winding of synchronous generators," *IEEE Transactions on Industrial Informatics*, 2021.

[14] J. Yun, S. B. Lee, M. Šašić, and G. C. Stone, "Reliable flux-based detection of field winding failures for synchronous generators," *IEEE Transactions on Energy Conversion*, vol. 34, no. 3, pp. 1715–1718, 2019.

[15] H. Ehya, A. Nysveen, I. Groth, and B. Mork, "Detailed magnetic field monitoring of short circuit defects of excitation winding in hydrogenerator," in *2020 International Conference on Electrical Machines (ICEM)*, vol. 1, pp. 2603–2609. IEEE, 2020.

[16] J. Yun, S. W. Park, C. Yang, S. B. Lee, J. A. Antonino-Daviu, M. Sasic, and G. C. Stone, "Airgap search coil-based detection of damper bar failures in salient pole synchronous motors," *IEEE Transactions on Industry Applications*, vol. 55, no. 4, pp. 3640–3648, 2019.

[17] I. Sadeghi, H. Ehya, and J. Faiz, "Analytic method for eccentricity fault diagnosis in salient-pole synchronous generators," in *2017 International Conference on Optimization of Electrical and Electronic Equipment (OPTIM) & 2017 Intl Aegean Conference on Electrical Machines and Power Electronics (ACEMP)*, pp. 261–267. IEEE, 2017.

[18] C. Jiang, S. Li, and T. G. Habetler, "A review of condition monitoring of induction motors based on stray flux," in *2017 IEEE Energy Conversion Congress and Exposition (ECCE)*, pp. 5424–5430. IEEE, 2017.

[19] G.-A. Capolino, R. Romary, H. Hénao, and R. Pusca, "State of the art on stray flux analysis in faulted electrical machines," in *2019 IEEE Workshop on Electrical Machines Design, Control and Diagnosis (WEMDCD)*, vol. 1, pp. 181–187. IEEE, 2019.

[20] J. A. Ramirez-Nunez, J. A. Antonino-Daviu, V. Climente-Alarcon, A. Lopez, H. Razik, R. A. Osornio-Rios, and R. d. J. Romero-Troncoso, "Evaluation of the detectability of electromechanical faults in induction motors via transient analysis of the stray flux," *IEEE Transactions on Industry Applications*, vol. 54, no. 5, pp. 4324–4332, 2018.

[21] I. Zamudio-Ramirez, J. A. Antonino-Daviu, R. A. Osornio-Rios, R. de Jesus Romero-Troncoso, and H. Razik, "Detection of winding asymmetries in wound-rotor induction motors via transient analysis of the external magnetic field," *IEEE Transactions on Industrial Electronics*, vol. 67, no. 6, pp. 5050–5059, 2020.

[22] P. A. Panagiotou, I. Arvanitakis, N. Lophitis, J. A. Daviu, and K. N. Gyftakis, "A new approach for broken rotor bar detection in induction motors using frequency extraction in stray flux signals," *IEEE Transactions on Industry Applications*, vol. 55, no. 4, pp. 3501–3511, 2019.

[23] P. Tian, J. A. ANTONINO-DAVIU, C. Platero, and L. D. Dunai, "Detection of field winding faults in synchronous motors via analysis of transient stray fluxes and currents," *IEEE Transactions on Energy Conversion*, 2020.

[24] M. F. Shaikh, J. Park, and S. B. Lee, "A non-intrusive leakage flux based method for detecting rotor faults in the starting transient of salient pole synchronous motors," *IEEE Transactions on Energy Conversion*, 2020.

[25] H. Castro-Coronado, J. Antonino-Daviu, A. Quijano-López, V. Fuster-Roig, and P. Llovera-Segovia, "Evaluation of the detectability of damper cage damages in synchronous motors through the advanced analysis of the stray flux," in *2020 IEEE Energy Conversion Congress and Exposition (ECCE)*, pp. 2058–2063. IEEE, 2020.

[26] B. Kedjar, A. Merkhouf, and K. Al-Haddad, "Large synchronous machines diagnosis based on air-gap and stray fluxes-an overview," in *2020 International Conference on Electrical Machines (ICEM)*, vol. 1, pp. 1384–1389. IEEE, 2020.

[27] M. Cuevas, R. Romary, J.-P. Lecointe, F. Morganti, and T. Jacq, "Noninvasive detection of winding short-circuit faults in salient pole synchronous machine with squirrel-cage damper," *IEEE Transactions on Industry Applications*, vol. 54, no. 6, pp. 5988–5997, 2018.

[28] ANSYS-Electronics®, Release 2019 R3.7, ANSYS, Inc.

[29] C. Torrence and G. P. Compo, "A practical guide to wavelet analysis," *Bulletin of the American Meteorological society*, vol. 79, no. 1, pp. 61–78, 1998.

[30] H. Ehya, A. Nysveen, and R. Nilssen, "Pattern recognition of inter-turn short circuit fault in wound field synchronous generator via stray flux monitoring," in *2020 International Conference on Electrical Machines (ICEM)*, vol. 1, DOI 10.1109/ICEM49940.2020.9270986, pp. 2631–2636, 2020.

[31] H. Ehya and A. Nysveen, "Pattern recognition of inter-turn short circuit fault in a synchronous generator using magnetic flux," *IEEE Transactions on Industry Applications*, DOI 10.1109/TIA.2021.3072881, pp. 1–1, 2021.

[32] H. Ehya, A. Nysveen, and T. N. Skreien, "Performance evaluation of signal processing tools used for fault detection of hydro-generators operating in noisy environments," *IEEE Transactions on Industry Applications*, DOI 10.1109/TIA.2021.3078136, pp. 1–1, 2021.

Hossein Ehya (S'19) received the M.Sc. degree in electrical engineering from the Department of Electrical and Computer Engineering, University of Tehran, Tehran, Iran, in 2013. From 2013 to 2018, he worked as an electrical machine design engineer in electrical machine companies.

He is currently working toward the Ph.D. degree in electrical engineering at the Norwegian University of Science and Technology (NTNU), Trondheim, Norway. In 2020, he was awarded with the ICEM Jorma Luomi Award in Gothenburg, Sweden. His research interests include the design and condition monitoring of electrical machines, signal processing, pattern recognition, and machine learning.

Arne Nysveen (M'98-SM'06) received his Dr. ing. degree (PhD) and his MSc in electric power engineering from the Norwegian Institute of Technology (now NTNU), Trondheim, Norway, in 1994 and 1988, respectively.

From 1995 to 2002, he was a Senior Scientist with ABB Corporate Research, Oslo, Norway. Since 2002, he has been a Professor at the Norwegian University of Science and Technology (NTNU), Trondheim. He is currently manager for the research on Turbine and Generator Technologies at the Norwegian Research Center for Hydropower Technology (HydroCen). His current research activities are on design, modelling and monitoring of hydroelectric generators.

Jose Antonino-Daviu (S'04, M'08, SM'12) received the M.Sc. and Ph.D. degrees in electrical engineering, both from the Universitat Politecnica de Valencia, Valencia, Spain, in 2000 and 2006, respectively. He has worked for IBM, involved in several international projects. He is currently a Full Professor in the Department of Electrical Engineering, Universitat Politecnica de Valencia. He was an Invited Professor at Helsinki University of Technology, Finland, in 2005 and 2007, Michigan State University, USA, in 2010, Korea University, South Korea, in 2014, Universite Claude Bernard Lyon 1, France, and Coventry University, U.K., in 2016. He is a coauthor of more than 200 papers published in technical journals and conference proceedings. He is also the coauthor of one international patent.

Dr. Antonino-Daviu is an Associate Editor of the IEEE Transactions on Industrial Informatics, IEEE Industrial Electronics Magazine and IEEE Journal of Emerging and Selected Topics in Industrial Electronics. He received the IEEE Second Prize Paper Award of the Electric Machines Committee of the IEEE Industry Applications Society (2013). He also received the Best Paper Award in the conferences IEEE ICEM 2012, IEEE SDEMPED 2011 and IEEE SDEMPED 2019 and the 'Highly Commended Recognition' of the IET Innovation Awards in 2014 and in 2016. He was the General co-Chair of SDEMPED 2013 and is a member of the steering committee of IEEE SDEMPED. In 2016, he received the Medal of the Spanish Royal Academy of Engineering (Madrid, Spain) for his contributions in new techniques for predictive maintenance of electric motors. In 2018, he has been awarded with the prestigious 'Nagamori Award' from the Nagamori Foundation (Kyoto, Japan). In 2019, he received the SDEMPED diagnostic achievement Award (Toulouse, France) for his contributions to electric motors advanced diagnosis.